Anisotropic Electron Spin Resonance Spectra of PCl_2 and NCl_2 in Low Temperature Matrices

MICHAEL S. WEI* AND JERRY H. CURRENT†
Department of Chemistry, University of Michigan, Ann Arbor, Michigan 48104
AND
JULIEN GENDELL
Department of Chemistry, Oakland University, Rochester, Michigan 48063

(Received 12 April 1971)

Well-resolved ESR spectra of PCl_2 were observed from the thermolysis (1000°C) of PCl_3, in argon, krypton, xenon, and nitrogen matrices. Satisfactory computer simulated spectra were obtained using two slightly different interpretations. One assumed a rhombic g tensor and an axially symmetric phosphorus hyperfine tensor; $g_{xx}=2.0024$, $g_{yy}=2.0011$, $g_{zz}=1.9962$; $C_{||}(P)=293$ G; $C_{\perp}(P)=\pm 30.5$ G; $C_{||}(Cl)=17.5$ G; $C_{\perp}(Cl)<0.3$ G. The other assumed an axial g tensor and a rhombic phosphorus hyperfine tensor; $g_{||}=2.0024$, $g_{\perp}=1.9986$; $C_{xx}(P)=293$ G; $C_{yy}(P)=\pm 39.0$ G; $C_{zz}(P)=\pm 22.5$ G; $C_{||}(Cl)=17.5$ G; $C_{\perp}(Cl)<0.3$ G. *In situ* photolysis of PCl_3 in argon produced a spectrum tentatively assigned to the asymmetric PClCl radical. The ESR spectrum due to NCl_2 radicals was observed from a direct room temperature spray-on of NCl_3 mixed with nitrogen or argon. Experiments using $^{15}NCl_3$ were also performed. The following assignment was obtained: $g_{xx}=2.006$, $g_{yy}=2.025$, $g_{zz}=2.023$; $C_{xx}(^{14}N)=40$ G; $C_{yy}(^{14}N)=14$ G; $C_{zz}(^{14}N)=6$ G; $C_{||}(Cl)=24$ G; $C_{\perp}(Cl)=17$ G. A discussion of the spin density distribution in the nitrogen and phosphorus dihalide radicals (NF_2, NCl_2, PF_2, and PCl_2) and of the electronic structure of these species using the available experimental data, atomic electronegativities, and the results of extended Hückel molecular orbital calculations is presented. Some information on the decomposition reactions of NCl_3 was obtained. A test of the reference values of the atomic nuclear moment—valence electron spin coupling parameters is possible by using the total spin densities determined for these radicals. The reference values calculated by Hurd and Cooden are shown to be preferable.

I. INTRODUCTION

The anisotropic electron spin resonance spectra of several nitrogen and phosphorus dihalides have been reported. Kasai and Whipple[1] analyzed the ESR spectrum of NF_2 in neon matrix at 4°K. Wei, Current, and Gendell[2] have reported the analysis of PF_2 in several rare gas matrices.

Nelson, Jackel, and Gordy[3] have recently reported the spectrum of PF_2 in xenon matrices. The anisotropic ESR spectrum of PCl_2 formed by the mercury lamp photolysis of PCl_3 in a frozen mixture of PCl_3 and PF_3 was reported by Kokoszka and Brinckman.[4] In this work, better resolved spectra of PCl_2 in inert gas matrices were obtained by the thermolysis of PCl_3. The previously unknown ESR spectra of NCl_2 and the nitrogen-15 substituted NCl_2 are also obtained. The molecular parameters from these four isostructural radicals (NF_2, PF_2, NCl_2, PCl_2) are used as a test of the applicability of extended Hückel molecular orbital calculations to simple inorganic radicals. The data may prove to be useful for comparison with results of other more sophisticated calculations. An empirical correlation of the unpaired electron distribution and electronegativity is also found.

II. EXPERIMENTAL TECHNIQUES

The cold temperature cell, the spectrometer, and the experimental techniques previously described[2] were used in this work.

Ultrahigh purity argon and nitrogen were obtained from the Matheson Company, Ltd. Research grade krypton, xenon, carbon dioxide, and sulfur hexafluoride were obtained from the same company. SF_6 was vacuum distilled through a liquid nitrogen bath to get rid of traces of air and other impurities. No purification was used for the other gases. Reagent grade PCl_3 was obtained from Mallinckrodt Company and distilled *in vacuo* over a CCl_4 slush bath (−23°C) into a liquid nitrogen bath. The lower boiling point portion was used.

NCl_3 was prepared[5] by passing chlorine gas, together with an inert carrier gas, through a solution of $(NH_4)_2SO_4$ in H_2SO_4. $^{15}NCl_3$ was prepared by the same method using 99.4% isotopic pure $(^{15}NH_4)_2SO_4$ obtained from International Chemical and Nuclear Corporation.

The computer programs used for spectra simulation, g-value calculations, and extended Hückel molecular orbital calculations have been described previously.[2,6] In some of the computer simulated ESR spectra regular oscillations were observed, e.g., see region ω in Fig. 3. These oscillations are due to the use of an insufficient number of angular orientations in the computation. They are an artifact of the computation which does not modify that part of the calculated spectrum corresponding to a significant ESR signal. They can be eliminated by either increasing the linewidth or by using a smaller spacing between θ and ϕ values. An extremely narrow line width, 0.6 G, is required to reproduce the resolution observed in the experimental spectrum; increasing the number of angular orientations would result in quite long computation times for a system with rhombic symmetry.

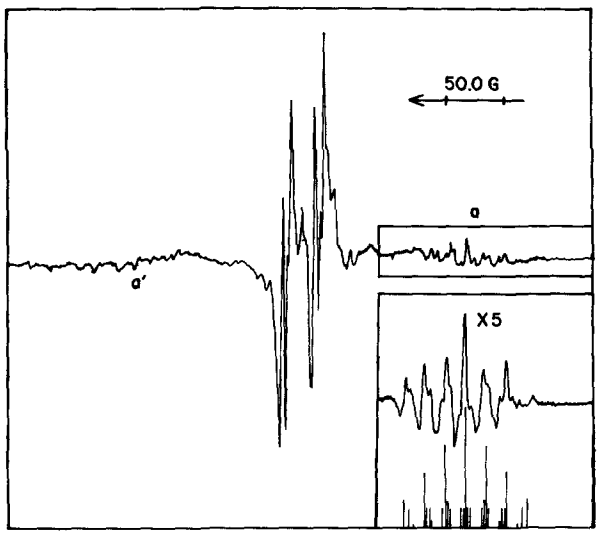

FIG. 1. ESR spectrum of PCl_2 in an argon matrix.

III. PCl_2

PCl_2 radicals were generated by passing a premixed sample of PCl_3 in argon ($M/R \simeq 500$) over a heated tungsten wire spot-welded in the cold temperature cell. No ESR signals were detected until the gaseous mixtures were heated to 1000°C, as measured by the simple Wheatstone bridge circuit. The ESR spectrum of PCl_2 in an argon matrix is shown in Fig. 1.

The thermolysis of PCl_3 was also studied in several other matrices, (Kr, Xe, N_2, and SF_6). Except for the broadening of certain spectral lines, rather similar spectra were produced in krypton, xenon, and nitrogen matrices. SF_6 was used as a matrix in a further attempt to observe an isotropic ESR spectrum. However, no ESR spectrum of PCl_2 was observed in the SF_6 matrix by the hot wire method. A few weak signals were observed in the $g=2$ region. This could be due to inefficient isolation in the matrix formed from heated SF_6 or reaction of the radical with the SF_6 matrix, or impurities present in the matrix.

In situ photolysis experiments in the various matrices were also performed. The results ranged from no ESR signal observed in a nitrogen matrix to a completely different spectrum in an argon matrix (see Sec. III.C). The spectra obtained by the photolysis of PCl_3 in krypton, xenon, and SF_6 matrices resembled those obtained in the thermolysis experiments.

A. Analysis of the PCl_2 Spectrum

The spectrum shown in Fig. 1 is believed to be due to PCl_2 radicals. With the low spray-on rate (1500 cc·cm/h) and the fast pumping rate of the cryogenic surface, an extremely low pressure could be attained in the cell. The mean free path of the PCl_3 molecule beyond the needle valve in the spray-on line was the order of meters, and the hot filament was less than 2 cm away from the cold window, thus secondary radical molecule reactions were extremely unlikely. A one-step mechanism for the thermal decomposition of PCl_3 is therefore highly favored. The paramagnetic decomposition products of PCl_3 are the PCl_2 and PCl radicals, and the phosphorus and chlorine atoms. PCl should have a $^3\Sigma$ ground state as have O_2 and PF,[7] so it is not likely to give an ESR spectrum when trapped in a matrix despite its paramagnetic character. The ESR spectrum of halogen atoms in the gas phase[8] has been observed but attempts to detect halogen atoms in nonpolar matrices have been unsuccessful.[9]

A small amount of phosphorus atom (<10% of total paramagnetic species observed) was detected in an argon matrix on the thermolysis of PCl_3. Figure 2(b) shows the high resolution spectrum of PCl_2 in an argon matrix (perpendicular region only). The spectrum indicates six lines; two of these lines, marked *P*, are due to phosphorus atoms. By increasing the klystron power, these lines are saturated more readily than the others. The *g* value and hyperfine splitting were found to be 2.0015 and 29.3 G, respectively. The ESR spectrum of phosphorus atoms, formed by the uv lamp photolysis of PH_3 in argon and krypton matrices at 4°K has been reported.[10] In the krypton matrix, a *g* value of 2.0027 and a hyperfine coupling of 30.5 G were reported. In the argon matrix, the phosphorus hyperfine splitting was 29.5 G; the *g* value was not reported.

We have repeated the above photolysis experiment of PH_3 in the argon matrix at 20°K. The phosphorus atoms thus produced have the same *g* and hyperfine values (2.0013 and 29.0 G) to within experimental error as the ones obtained by the thermolysis experiments (2.0015 and 29.3 G).

The assignment of the PCl_2 spectrum is partially based on the assumption that the radicals are slightly preferentially oriented with their molecular plane along

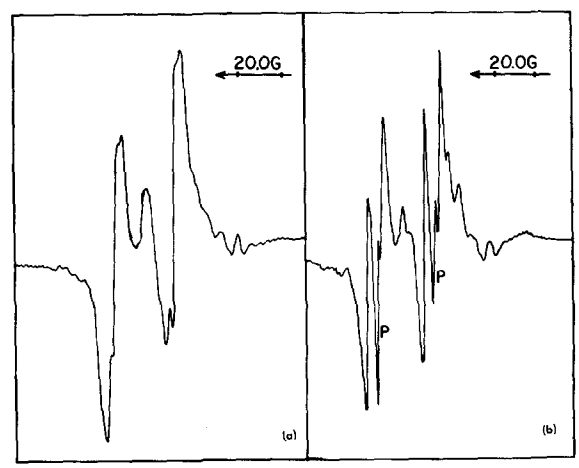

FIG. 2. ESR spectra of PCl_2 (perpendicular regions only) (a) in a nitrogen matrix (b) in an argon matrix.

the surface of the matrix.[11,12] Upon rotation of the cold window with respect to the external field, the intensities of the peaks marked a and a' in Fig. 1 increased by ~50%. They are therefore designated as the parallel components. The other lines are the perpendicular features and are essentially unaffected by rotating the sample.

The thermolysis products of PCl_3 isolated in other matrices (N_2, Kr, and Xe) yielded essentially the same spectrum as in argon matrix. However, the spectral lines were in general very much broadened. The perpendicular components were broadened so that an apparent axial symmetry was observed, and the phosphorus atom lines were completely obscured. As an illustration of this broadening effect in different matrices, the spectra of PCl_2 (perpendicular region only) in nitrogen and argon matrices are shown in Fig. 2.

The assignment of the PCl_2 spectrum was confirmed by the computer simulation method (Fig. 3). The computer program for PF_2 was modified to[2] allow for spin $\frac{3}{2}$ nuclei so that for each orientation of the radical with respect to the field, the resonance line was split into four components rather than two components as in the spin $\frac{1}{2}$ system. Second-order corrections due to chlorine nuclei were not included in the program because the chlorine hyperfine splittings were found to be quite small. In the X-band frequency range this second-order effect would amount to less than a fraction of a gauss. However, the second-order splitting due to phosphorus could not be ignored. The same formulation as in PF_2 [2] and CF_3 [13] was used in this case.

The well-resolved ESR spectrum of PCl_2 (Figs. 1 and 2) has enabled us to assign the phosphorus and chlorine hyperfine splittings. The chlorine perpendicular splitting is found to be less than 0.3 G. Since the experimental linewidth (measured as half the peak-to-peak distance) of the perpendicular component is in the order of ~0.5 G, a computer simulation with a chlorine $\perp$ splitting greater than 0.3 G results in a broader linewidth than the experimental ones.

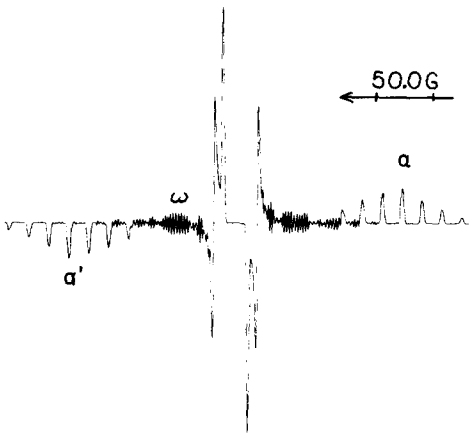

FIG. 3. Computer simulated spectrum of PCl_2. The parameters are the experimental values for an argon matrix, PCl_2 (A), given in Table I.

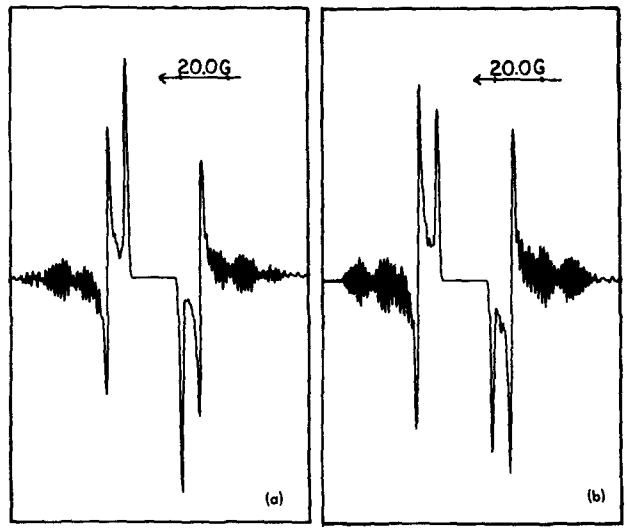

FIG. 4. Computer simulated spectra of PCl_2 in an argon matrix (perpendicular regions only) using the two interpretations discussed in Sec. III.A. The parameters are given in Table I (a) rhombic g tensor, $PCl_2(A)$ and (b) rhombic phosphorus hyperfine tensor, $PCl_2(B)$.

If the g and hyperfine tensors have axial symmetry, only two lines should be observed in the perpendicular region. Under lower resolution, as in Kokoszka and Brinckman's[4] work, only one broad line could be detected. Our experimental spectra show four distinct sharp lines in the perpendicular region. This indicates that the g tensor and/or phosphorus hyperfine tensor has rhombic symmetry.

Figure 4 shows computer simulated spectra for the perpendicular region of PCl_2: In the first case (Spectrum A), the g tensor is rhombic and the phosphorus hyperfine tensor is axial; in the second case (Spectrum B), the g tensor is axial and the phosphorus hyperfine tensor is rhombic. Other than small changes in intensity ratios, the computer simulated spectra for these two calculations are essentially identical. The parameters used for these two cases are given in Table I.

It is not possible to choose between these interpretations since the microwave frequency could not be changed sufficiently to reveal a g value difference. g tensor calculations using eigenvectors and eigenvalues from extended Hückel calculations indicate that the g tensor is likely to be rhombic. On the other hand, the deviation from axial symmetry of the phosphorus hyperfine tensor is small, less than 5%. Bond polarization[14,15] and inner shell polarization[16] have been known to produce such effects.

Our experimental values are somewhat different from the ones reported by Kokoszka and Brinckman[4] (see Table I). The differences in the components of the

TABLE I. Experimental g and hyperfine tensors for PCl_2, PClCl, and NCl_2.

Species	Matrix	g Value[a]			Hyperfine tensors[b] (G) P or N			Cl		Linewidth (G)[c] ($\perp$ component)
		$g_{\parallel}$	$g_{\perp}$	$g_{\perp}'$	$C_{\parallel}$	$C_{\perp}$	$C_{\perp}'$	$C_{\parallel}$	$C_{\perp}$	
$PCl_2(A)$[d]	Ar	2.0024	2.0011	1.9962	293	−30.5		17.5	<0.3	0.5
$PCl_2(B)$[d]	Ar	2.0024	1.9986		293	−39.0	−22.5	17.5	<0.3	0.5
PCl_2	Kr	...[e]	1.999		...[e]	−30		...[e]	<0.5	2.5
PCl_2	Xe	2.000	1.998		294	−28		16.0	<0.5	5.0
PCl_2	N_2	2.0024	1.999		293	−30		17.5	<0.5	3.0
PCl_2	SF_6	...[e]	1.998		...[e]	−30		...[e]	<0.5	6.0
PCl_2[f]	PCl_3/PF_3	2.001	2.017		269	−28		14.8	~0	
PClCl[g]	Ar	2.002	1.9995		263	−17.5	−13	9.0	−17.5; 0.0	0.5
$^{14}NCl_2$	Ar	2.006	2.023	2.026	40	14	6	24.0	−17.0	0.5

[a] Including second-order correction.

[b] The choice of signs for the hyperfine tensor components is discussed in Sec. V.A.

[c] The linewidth is $\frac{1}{2}$ (peak separation of the derivative shape).

[d] The two different sets of parameters, A and B, for PCl_2 in Ar is discussed in Sec. III.A.

[e] Value not determined.

[f] See Ref. 4.

[g] The spectrum observed when PCl_3 is photolyzed in an argon matrix is tentatively assigned to asymmetric PClCl with the two chlorine atoms having different values of $C_{\perp}$ as indicated.

hyperfine tensors may be due to (a) experimental error in determining line positions and (b) matrix effects which cause a large change in $C_{xx}(P)$, but even this change of 24 G is not unreasonable. Their observed value of $g_{\perp}=2.017$ (corrected for second-order effects) differs greatly from our value of 1.9986. This could also be due to a matrix effect since they used a matrix of PCl_3 and PF_3 but the shift is unusually large. The unresolved perpendicular components in their spectra may also be an indication of additional signals from unidentified radicals which could cause an apparent shift in $g_{\perp}$.

B. Linewidth and Matrix Effects

The PCl_2 radical was studied in other matrices mainly to confirm the assignment of the spectrum, and to study the somewhat anomalous behavior of the photolysis reaction. The results, tabulated in Table I, indicate that the same radicals were trapped in the different matrices but radical matrix interaction caused the spectral lines to be broadened in nitrogen, krypton, and xenon matrices. In krypton and xenon matrices, the parallel components were broadened to a point beyond detection.

In argon matrices, the parallel features are broader than the perpendicular features as was observed for PF_2.[2] The average linewidth of the parallel components are the order of 3 G (linewidth measured as $\frac{1}{2}$ (width at half-height), whereas the perpendicular components are only 0.5 G wide. To lower computer costs, a variable linewidth parameter was not used in the program. Instead this effect was simulated by summing three computer spectra, with the same phosphorus perpendicular hyperfine splitting but slight variations of the parallel splitting.

From the natural abundance of ^{35}Cl and ^{37}Cl, the probability ratio of $^{35}ClP^{35}Cl:{}^{35}ClP^{37}Cl:{}^{37}ClP^{37}Cl$ is approximately 9:6:1. The magnetic moment of ^{37}Cl is ~0.84 of that of ^{35}Cl and both nuclei have a spin of $\frac{3}{2}$. In the ESR spectrum of PCl_2, the perpendicular components of the chlorine hyperfine splitting is small, thus the isotope effect is not observed. The stick spectrum including the isotope effect for the parallel components is included in Fig. 1. Experimentally, the isotope effect was not resolved, but the line broadening and observed shoulders coincide with the expected isotopic line positions in a very satisfactory way.

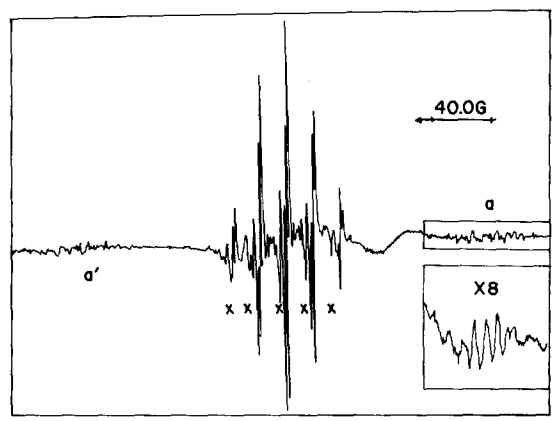

FIG. 5. ESR spectrum of asymmetric PClCl in an argon matrix.

C. Asymmetric PClCl Radical

Mercury lamp photolysis of deposited PCl_3 in argon ($M/R=1200$) resulted in a new ESR spectrum (Fig. 5) which is tentatively assigned to the asymmetric PClCl radical. The spectral regions marked a and a' in Fig. 5 are designated the parallel components; their intensities were observed to increase on rotating the sample. These regions are split by only 263 G (293 G was observed for symmetric PCl_2) and the components in each region have a 9.0 G spacing. The perpendicular region of this spectrum is also undoubtedly different from that of symmetric PCl_2. It is thus clear that a species different from the symmetric PCl_2 radical is produced in this experiment. A radical containing one phosphorus atom and two chlorine atoms is implied by the starting material and the structure of the parallel components.

The five major signals in the central region, each having further structure, are believed to be the perpendicular components. A five-line spectrum of intensity 1:2:2:2:1 is obtained if one spin $\frac{3}{2}$ nucleus and a spin $\frac{1}{2}$ nucleus have precisely the same hyperfine splitting constants. It is thus concluded that the perpendicular hyperfine splitting constants for one chlorine is much smaller than that of the other. A calculated spectrum using the parameters in Table I is shown in Fig. 6. Under higher resolution the structure of each of the five major signals in the central region can be separated into two groups, using linewidths as a criterion. One group has a narrower width and shows further structure, while the other group (indicated by x's in Fig. 5), which has much lower intensity, has a wider width, and is slightly displaced from the narrower group. We suggest that this could be due to asymmetric PClCl radicals residing in slightly different sites.

The mechanism for the formation of asymmetric PClCl is not understood. A single step or multiple step photolysis could be involved but these mechanisms do not explain why this radical is not observed when PCl_3 is photolyzed in nitrogen, krypton, or xenon. Due to the large linewidths in the krypton and xenon matrices, however, we cannot rule out the possibility that asymmetric PClCl is also formed in these matrices but is not detected.

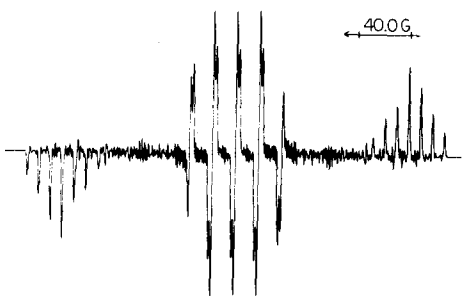

FIG. 6. Computer simulated spectrum of asymmetric PClCl. The parameters are given in Table I.

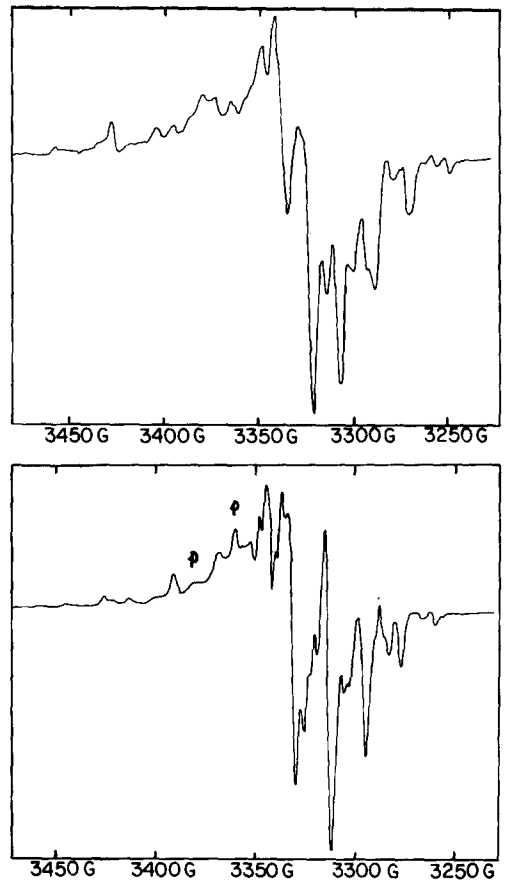

FIG. 7. ESR spectra of NCl_2 in an argon matrix under conditions of low resolution (see Sec. IV.A) upper, $^{14}NCl_2$; lower, $^{15}NCl_2$.

IV. NCl_2

Direct room temperature spray-on of NCl_3/Ar and NCl_3/N_2 in the usual slow manner onto the cold window gave intense ESR signals. The signals observed were probably due to the decomposition of NCl_3 as the gaseous mixture expanded into a vacuum. Again assuming no radical molecule reactions, the paramagnetic species observed were most likely due to NCl_2 radicals.

NCl_3 is a thermodynamically unstable molecule and has been known to undergo decomposition on expanding the gas into vacuum; the ultimate products being nitrogen and chlorine molecules.[17]

In the NCl_3 system, the only matrices used were nitrogen and argon. Identical low resolution spectra were obtained in both cases. It was possible, however, to obtain spectra with much better resolution in an argon matrix if the concentration of NCl_2 radicals was sufficiently low.

It was impossible to measure absolute molar concentration of NCl_3 in the spray-on mixture. Approximate concentrations were determined by the gas phase infrared absorbance. The M/R ratio was estimated to be about 100 for the most concentrated samples and 500 for the most dilute.

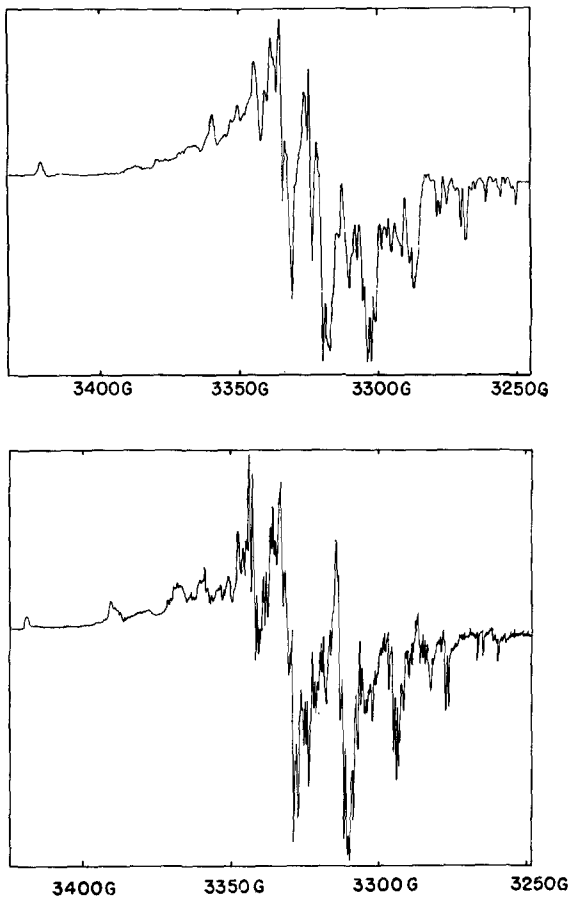

FIG. 8. ESR spectra of NCl_2 in an argon matrix under conditions of high resolution (see Sec. IV.A upper, $^{14}NCl_2$; lower, $^{15}NCl_2$.

Most of the experiments performed on NCl_3 have been repeated with $^{15}NCl_3$. The ESR spectra of $^{14}NCl_2$ and $^{15}NCl_2$ are shown in Figs. 7 and 8. For comparison purposes, the nitrogen-14 and nitrogen-15 spectra are put on the same figure. Unfortunately, the sweep rates on these spectra are not identical. Absolute field positions were calibrated for each spectrum.

A. Analysis of the NCl_2 Spectrum

In our analysis of the PF_2 [2] and PCl_2 spectra, the anisotropy in hyperfine tensors is much larger than the anisotropy in the g tensor. In the case of NCl_2, the spectrum is more complex, because the anisotropies for both the g and hyperfine tensors are of comparable magnitude. The g tensor anisotropy is apparent from the experimental spectra shown in Fig. 7. The total extent of the spectrum (associated with the parallel features) is symmetric about a g value (2.006) which is close to the free electron value. The most intense features are, however, centered at a considerably lower field value associated with a g value of approximately 2.02. These intense features are associated with the perpendicular axes. The general intensity characteristics are reproduced by all calculations which include this g anisotropy.

The parallel and perpendicular components are overlapped to the point that they are not easily resolvable. Rotation of the matrix with respect to the external field causes certain changes in line intensities which are observable in the high resolution spectra. However, due to the complexity of the spectra, the perpendicular and parallel components cannot be unambiguously determined by this method.

The ratio between the magnetic moment of nitrogen-15 and nitrogen-14 is 1.402. The spin of ^{15}N is $\frac{1}{2}$ and that of ^{14}N is 1. Thus, the isotopically substituted spectrum of NCl_2, using nitrogen-15, was extremely helpful in the analysis of the spectrum. The experimental spectra of $^{14}NCl_2$ and $^{15}NCl_2$ appeared to have the same general feature, but the field positions of the resonance lines are quite different (Figs. 7 and 8). A line separation of 17 G is observed in both the $^{14}NCl_2$ and $^{15}NCl_2$ spectra. Hence this splitting must be due to one of the components of the chlorine hyperfine tensor rather than a nitrogen tensor component.

The change in the extent of the spectrum on nitrogen isotopic substitution was used to estimate the value of

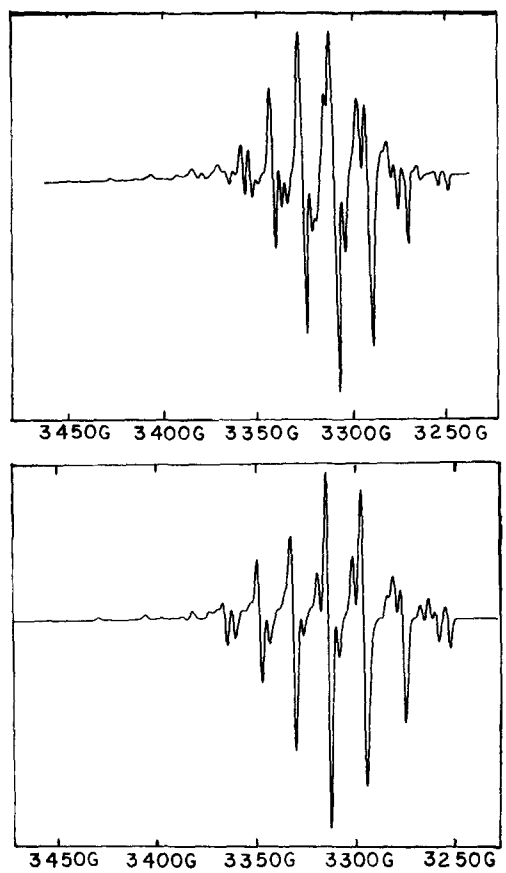

FIG. 9. Computer simulated spectra of NCl_2. The parameters for $^{14}NCl_2$ are given in Table I upper, $^{14}NCl_2$; lower, $^{15}NCl_2$.

$C_{||}(N)$. If we assume that the sum of the parallel hyperfine tensor components is larger than that of the perpendicular ones, the extent of the spectrum is defined by the parallel features. The spin of the chlorine nucleus is $\frac{3}{2}$, thus two equivalent chlorine nuclei would give seven equally spaced lines of intensity ratio 1:2:3:4:3:2:1. The nitrogen-14 nucleus gives three equally spaced lines. Thus the extent of the $^{14}NCl_2$ spectrum is $2C_{||}(^{14}N)+6C_{||}(Cl)$. Similarly, the extent of the $^{15}NCl_2$ spectrum is $C_{||}(^{15}N)+6C_{||}(Cl)$. Thus, from the ratio of the magnetic moments, $C_{||}(^{14}N)=0.71\ C_{||}(^{15}N)$, the difference of extent of these two spectra is $0.42\ C_{||}(^{15}N)$. Experimentally, this difference was found to be 23 *G*, thus $C_{||}(^{15}N)\simeq 55$ G, and $C_{||}(^{14}N)\simeq 39$ G.

Also, from the extent of the NCl_2 spectrum, the parallel component of the chlorine hyperfine tensor was found to be 24 G. The 17 G splittings are therefore assigned to the perpendicular chlorine hyperfine splittings. The perpendicular component of the nitrogen hyperfine tensor is the least well-defined parameter, and was determined by computer simulation using the trial and error method.

Since the hyperfine tensor components for both nitrogen and chlorine are rather small, (<60 G), second-order effects are small (<1 G) and are not included in the calculation. By assuming that the radicals have axially symmetric *g* and hyperfine tensors, reasonably good low resolution spectra were obtained with $C_{\perp}(^{14}N\simeq 14\pm 3$ G. A better fit for the high resolution spectra was obtained by assuming a nonaxial nitrogen hyperfine tensor and a nonaxial *g* tensor. The computer simulated spectra of $^{14}NCl_2$ and $^{15}NCl_2$ are shown in Fig. 9. The parameters used for $^{14}NCl_2$ are given in Table I. There is good agreement between the experimental and the calculated line positions. The major discrepancies are in line shapes especially in the low field region where both the extreme parallel and perpendicular lines fall. Matrix effects causing a site variation of parameters as in PCl_2 and PF_2 are likely to be present for NCl_2 as well. These two facts contribute to the difficulty of fitting line intensities in the low field region of the NCl_2 spectrum. In addition, there is some evidence that a small amount of other nitrogen- and chlorine-containing radicals are formed from the decomposition of NCl_3 (see Sec. IV.B). The fine structure in the high resolution spectra is apparently due to the chlorine isotopes and some deviation from axial symmetry for the chlorine hyperfine tensor.

B. Reactions of NCl_3

In one experiment, NCl_3/Ar was bled into the spray-on line (volume of line ~150 cc) until a total pressure of ~30 cm Hg was built up and spray-on was conducted in a different fashion. The needle valve was opened rapidly so that the sample was pulsed into the deposition chamber. Fast deposition rates are usually unfavorable for matrix isolation studies, because some of the matrix gases are not trapped on the cold window and localized melting may result. In this experiment, however, free nitrogen atoms as well as the NCl_2 radicals were detected. The nitrogen atoms were characterized by three lines (spin of $^{14}N=1$), the *g* value and hyperfine coupling constant are 2.0020 and 4.28 G, respectively.[18] Although only a small fraction of the N atoms could be isolated with these spray-on conditions, the sensitivity of ESR spectroscopy allowed them to be easily detected. The atoms, which would normally recombine on the walls of the spray-on line, were apparently swept in a laminar flow into the deposition chamber under fast flow conditions.

In the slow deposition experiments, a metal needle valve was used to regulate the spray-on rates. Photolysis of the samples in argon and nitrogen matrices, using an unfiltered mercury lamp ($\lambda>2100$ Å), produced nitrogen atoms but no other new species. When greaseless Teflon valves were used to regulate the flow, the same NCl_2 spectrum was observed at room temperature spray-on. However, upon photolysis, the nitrogen atom signal was orders of magnitude higher than when metal surfaces were present in the spray-on system.

Since the presence of metal surfaces only affected the nitrogen atoms produced on photolysis but not the NCl_2 radicals, it suggested that the nitrogen atom is a photolysis product of NCl_3 rather than NCl_2 and that metal surfaces also cause the decomposition of NCl_3.

Infrared experiments have shown that[19] NCl_3 is readily decomposed in metal spray-on lines but that it may be deposited with very little decomposition using a glass system with Teflon stopcocks. Extended photolysis of matrix isolated NCl_3 results in the destruction of all infrared absorbing species.[19] The rate of formation of nitrogen atoms was initially fast but reached a steady state concentration in approximately $\frac{1}{2}$ h. The NCl_2 signals were observed to decrease in intensity, until a steady state was reached in which approximately 80% of the original signal intensities were left. However, due to the complexity of the spectrum, it was not possible to perform an accurate photolysis rate study.

Burdett[19] suggested a one-step mechanism in which all N–Cl bonds in NCl_3 are fissioned on photolysis. To investigate this possibility, experiments were performed in which the matrix was doped with ~1% chlorine molecules. This was done in two ways: by adding gaseous chlorine molecules directly to the sample bulb, and by using a dual spray-on system. The dual spray-on experiments were performed by putting NCl_3 in Ar in one vacuum line and Cl_2 in Ar

TABLE II. Dipolar and isotropic components of the hyperfine tensors for radical species in argon (G).

Species	P or N				Cl or F			
	$B_{\|\|}$	$B_\perp$	$B_\perp'$	A_c	$B_{\|\|}$	$B_\perp$	$B_\perp'$	A_c
$PCl_2(A)$[a]	216	−107.5	−107.5	77.0	11.7	−5.8	−5.8	5.8
$PCl_2(B)$	216	−116.0	−99.5	77.0	11.7	−5.8	−5.8	5.8
PClCl[b]	185.5	−95.0	−90.5	77.5	17.7	−8.8	−8.8	−8.7
					6.0	−3.0	−3.0	3.0
$^{14}NCl_2$	20.0	−6.0	−14.0	20.0	27.3	−13.7	−13.7	−3.3
PF_2[c]	260	−130	−130	47.0	62.0	−31.0	−31.0	65.0
NF_2[d]	32	−16	−16	16	152	−76	−76	59

[a] $PCl_2(A)$ and $PCl_2(B)$ refer to the two sets of parameters in Table I.
[b] The two sets of chlorine values are due to the nonequivalence of the chlorine atoms in this species.
[c] See Ref. 2.
[d] See Ref. 1.

in another. The samples were then sprayed on simultaneously. Because of the design of the cold temperature cell, the gaseous streams were allowed to mix when they were ~2 cm from the cold window. In either experimental setup, the results were essentially identical. The same NCl_2 spectrum was produced at room temperature spray-on. Upon photolysis, nitrogen atoms were produced as before but in addition the peaks marked *P* in Fig. 7 were found to increase in intensity. Thus the lines marked *P* are likely to be due to some other nitrogen- and chlorine-containing radical species—possibly asymmetric NClCl or NCl_4. Infrared studies have suggested that the asymmetric NClCl radical[19] is one of the photolysis products of NCl_3 in argon matrices doped with chlorine molecules.

V. DISCUSSION

A. Signs of the Hyperfine Components; Determination of Spin Densities

Estimates of the unpaired electron spin densities on each atom of the radical species can be obtained by first resolving the hyperfine coupling tensors, **C**, into an isotropic part A_c and a dipolar part **B** ($\mathbf{C}=A_c\mathbf{U}+\mathbf{B}$, where **U**=unit tensor), and then using the approximation that the *p*-orbital spin density is given by $B_{\text{exptl}}/B_{\text{ref}}$ where (1) B_{exptl} is the value of the positive component of the anisotropic hyperfine tensor which is symmetric about the *p*-orbital axis and, (2) B_{ref} is the corresponding value calculated for an isolated atom.[2,20] The signs of the **C** tensor principal values cannot be determined directly from the experiments which were performed. However, for each of the radicals studied in this work, the unpaired electron is in a molecular orbital of b_1 symmetry consisting of an antibonding combination of p_x orbitals on the three atoms (the *x* axis is perpendicular to the molecular plane).[2] Thus, for each radical B_{xx} or $B_{||}$ should have a positive value and the **B** tensors should have close to axial symmetry about the *x* axis. These criteria eliminate many of the sign possibilities for the hyperfine components but do not result in an unambiguous assignment. For PF_2 and NF_2 the isotropic values have been determined experimentally[21,22] and the signs used in Table I have been chosen to give agreement with these values. Isotropic values for PCl_2 and NCl_2 have not yet been measured experimentally.

In the case of NCl_2, we feel that a definitive choice of the signs of all hyperfine components can be made on the basis of the following qualitative argument: When the data from NF_2 and PF_2 were compared,[2] it was observed that the spin density on the fluorine atoms in PF_2 is less than that on NF_2. It was argued that the difference in electronegativities between fluorine and the central atom must operate so as to localize the unpaired electron mainly on the central atom and, since phosphorus is more electropositive than nitrogen, this effect should be larger in PF_2 than in NF_2. The same argument should apply equally to a comparison of PCl_2 and NCl_2: Namely, the spin density on the chlorine atoms in PCl_2 should be less than that on NCl_2. Since for PCl_2, $C_\perp(\text{Cl})$ is about zero the sign of $C_{||}(\text{Cl})$ must be positive and a definite value for the chlorine spin density in PCl_2 can be determined. There is only one choice of signs for the chlorine components in NCl_2 which results in a larger spin density for chlorine in NCl_2 than in PCl_2 and this assignment is given in Table I. An analogous argument to the one given above for the comparison of the chlorine spin densities in PCl_2 and NCl_2 should apply to the comparison of the nitrogen spin densities in NCl_2 and NF_2: Namely, the nitrogen spin density in NF_2 should be larger than that in NCl_2. Only the assignment of nitrogen hyperfine components given in Table I is consistent with this relationship. Thus, we feel that the signs of all the hyperfine components for NF_2, PF_2, and NCl_2 are known, but that some

TABLE III. p-Orbital spin densities.

Species	Experimental[a]		Calculated[b]		Total[c]	Normalized[d]
	P or N	Cl or F	P or N	Cl or F		P or N
$PCl_2(A)$[e]	0.82	0.095	0.80	0.10	1.01	0.81
$PCl_2(B)$	0.84	0.095			1.03	0.81
PClCl[f]	0.71	0.14; 0.05	0.77	0.21; 0.03	0.90	0.79
$^{14}NCl_2$	0.57	0.22	0.57	0.215	1.01	0.57
PF_2	0.99	0.05	0.88	0.06	1.09	0.91
NF_2	0.80	0.12	0.76	0.12	1.04	0.77

[a] Values obtained from experimental data as described in Sec. V.A.
[b] Results of extended Hückel calculations see Sec. V.B.
[c] Sum of experimental spin densities.
[d] Spin density normalized to one electron see Sec. V.B.
[e] $PCl_2(A)$ and $PCl_2(B)$ refer to the two sets of parameters in Table I.
[f] The calculations yield the result that the chlorine atom bonded to the phosphorus has the higher spin density.

ambiguity still remains regarding the signs of some of the perpendicular components for both symmetric and asymmetric PCl_2.

Some additional evidence which indicates the choice of signs in the remaining cases can be obtained by looking at the actual magnitudes of the spin densities. The hyperfine tensors **C** have been decomposed into isotropic and anisotropic parts as described above and these hyperfine components are given in Table II. To a first approximation, as discussed above, **B** should be axially symmetric. However, bond polarization[14,16] and inner-shell spin polarization[16] can cause **B** to deviate from axial symmetry (the same effects, of course, produce nonzero values for the isotropic components). For the nonaxial case, **B** can be resolved into two axially symmetric tensors $\mathbf{B}_1$ and $\mathbf{B}_2$; $\mathbf{B}=\mathbf{B}_1+\mathbf{B}_2$. The hyperfine tensor, $\mathbf{B}_1$, which is symmetric about the x axis is due to the unpaired electron in a molecular orbital of b_1 symmetry. This unpaired electron polarizes, for example, the $4a_1$ molecular orbital, which contains p_z and s character resulting in the dipolar tensor, $\mathbf{B}_2$, with small principal values compared to those of $\mathbf{B}_1$. For the phosphorus hyperfine tensor in PCl_2 (in the case where the perpendicular components are chosen to be negative), the principal values of $\mathbf{B}_1$ are (221.3, -110.7, -110.7) and for $\mathbf{B}_2$ they are (-5.3, -5.3, 10.7). The small values for $\mathbf{B}_2$ indicating a small amount of polarization. In the case of NCl_2, polarization effects are apparently somewhat larger. Here $\mathbf{B}_1=(22.7, -11.3, -11.3)$ and $\mathbf{B}_2=(-2.7, -2.7, +5.4)$. In the cases of rhombic **B** tensors, the p_x spin density is calculated from the positive component of $\mathbf{B}_1$ as the ratio $B_{\text{exptl}}/B_{\text{ref}}$ since it is the tensor $\mathbf{Y}_1$ which is related to the unpaired spin density in the p_x orbital.

The reference values used in the calculations of spin densities are those reported by Hurd and Coodin.[23] The reasons for using this set of values rather than some other set are given in the Appendix. Spin densities determined in this manner from the experimental data are listed in Table III. For all the symmetric Group V dihalides, the total spin densities are close to the value unity, representing one unpaired electron for the radical. If the perpendicular components of PCl_2 are chosen to be positive, instead of negative as was done in Table I, the phosphorus spin density is lowered from 0.82 to 0.67 and the total spin density is lowered from 1.01 to 0.86. Thus if a positive assignment is used, the total spin density for PCl_2 is considerably lower than the corresponding quantity for the other radicals and this argues for the negative assignment made in Table I. There is essentially no difference in the spin density distribution for PCl_2 with an axial or a rhombic hyperfine tensor so this question is still an open one.

For asymmetric PClCl, the uncertainty in the signs of the perpendicular components for phosphorus and chlorine were decided in favor of the negative values used in Table I on the basis of the magnitude of the total spin density as in the case of symmetric PCl_2. The negative assignment in Table I gives 0.90 for the total spin density while other assignments result in significantly lower values for this quantity.

B. Hückel MO Calculations

Extended Hückel MO calculations were made on PCl_2 and NCl_2 in the same manner as previously conducted for PF_2 and NF_2.[2] A more detailed description of this type of calculation has recently been published by Bartell *et al.*[24] The ionization potentials and Slater exponents which were used are tabulated in Table IV. The bond length used for PCl_2 was 2.04 Å, the same as that in PCl_3,[25] and since the calculations were rather insensitive to small changes in bond angle, an arbitrary angle of 104° was used. (The bond angle of PCl_3 is 100°6′.[25])

TABLE IV. Orbital parameters used in extended Hückel calculations.[a]

Atom	Atomic orbital	Orbital exponent	Diagonal matrix element (electron volts)
Nitrogen	2s	1.950	−28.13
	2p	1.950	−14.54
Oxygen	2s	2.275	−35.13
	2p	2.75	−13.62
Fluorine	2s	2.600	−42.51
	2p	2.600	−17.42
Phosphorus	3s	1.600	−20.30
	3p	1.600	−11.00
	3d	1.100	−2.50
Chlorine	3s	2.033	−24.02[b]
	3p	2.033	−15.03[b]
	3d	1.300	−2.50

[a] See Ref. 24.
[b] J. Hinze and H. H. Jaffé, J. Am. Chem. Soc. **84**, 540 (1961).

Since the geometry of the asymmetric PClCl radical is unknown, the chlorine–chlorine bond distance was assumed to be the same as in the Cl_2 molecule and the phosphorus–chlorine distance was that in PCl_3. Variations of the P–Cl bond length showed no significant change in the total energy.

A series of calculations were performed on the asymmetric PClCl radical, varying the bond angle from 90° to 180°. A minimum total energy and a maximum bond overlap population were found at an angle of 120°. This value of the bond angle was used in the calculation of spin densities. Similar calculations were performed on the O_2F radical, and the results were in fair agreement with the experimental value, 110°. To perform the extended Hückel MO calculations for NCl_2, the bond angle and bond length were chosen as 106° and 1.73 Å, respectively, as in CH_3NCl_2.[26] Calculated spin densities are listed in Table III and there is generally excellent agreement between experimentally determined and calculated values. This agreement should be treated with some reservation, however, since the calculated spin density distribution depends on the magnitude of the valence state ionization potentials.

For asymmetric PClCl, it is impossible experimentally to assign the sets of chlorine hyperfine tensors to their corresponding nuclei. However, the extended Hückel MO calculations indicate that the unpaired electron is localized to a higher extent on the central chlorine atom than the terminal one. The experimental and calculated spin densities are in good agreement with each other. Spin densities normalized to one electron give perhaps a slightly better indication of the relative spin density on the phosphorus or nitrogen atom.[2,4] These values are also listed in Table III.

C. Electronegativities and Spin Densities

An empirical model can be used to correlate spin densities with electronegativities. The more electronegative atoms are said to attract the bonding electrons, thus for these 19-electron radicals in which the unpaired electron is antibonding, the unpaired spin density should be large on atoms having relatively small electronegativities (see Sec. IV.A and Ref. 2).

Atkins and Symons[20] and Bower, Symons, and Tinling[27] have made correlations of spin densities and electronegativities for certain 17-, 19-, and 25-electron radicals. Their results were rather uncertain for the following reasons: (1) The radicals they investigated (SeO_2^-, CO_2^-, NO_2, NO_2^{-2}, ClO_2) contained only one magnetic nucleus. (2) Their correlation included both 17- and 19-electron radicals. We feel that this is improper because in the case of 17-electron radicals, the odd electron is in a bonding orbital whereas for 19-electron radicals, it is in an antibonding orbital. This would produce opposite effects as far as electronegativities are concerned.

All the atoms in the Group V dihalides have magnetic moments, thus the spin density distribution can be determined to a high degree of accuracy. Also, these radicals all have 19 valence electrons. Figure 10 shows a plot of the normalized spin density on the central atom vs one-half the difference in electronegativity between the Group V atom and the halogen, using Pauling's electronegativity[28] scale. The smooth functional relationship exhibited in Fig. 10 is encouraging. It would be desirable to have more experimental data to verify this simple correlation.

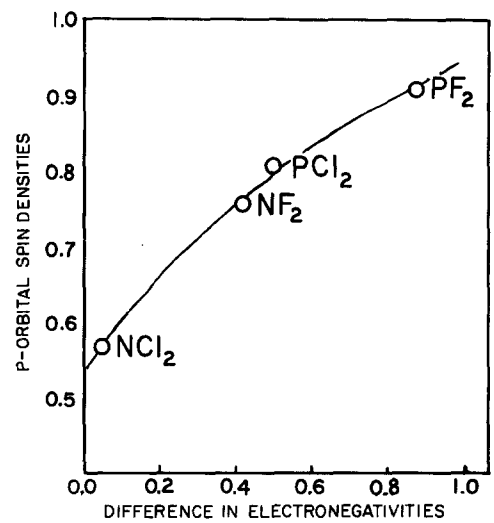

FIG. 10. Normalized p-orbital spin densities on the central atom (Table III) vs one-half the difference in electronegativity between the central atom and the halogen atoms (see Sec. V.C).

The normalized spin density on the phosphorus atom for asymmetric PClCl is very close to that in symmetric PCl_2; therefore, asymmetric PClCl would also fit on the curve in Fig. 10. The fact that the spin densities are approximately the same for symmetric and asymmetric PCl_2 may be fortuitous but it is consistent with the molecular orbital description of 19-electron radicals.

D. g Values

The experimentally determined g values (corrected for second-order effects) for PF_2, PCl_2, NF_2, and NCl_2 are given in Table I. Calculated g values, using atomic orbitals and orbital energies from the extended Hückel calculations, for PF_2 and NF_2 have been previously reported.[2] Similar calculations for PCl_2 and NCl_2 were made with the following results: PCl_2, $g_{xx}=2.0020$; $g_{yy}=2.0024$; $g_{zz}=2.0034$; NCl_2, $g_{xx}=2.0060$; $g_{yy}=2.1460$; $g_{zz}=2.1114$. It should be noted that in the axis system we have used,[2] the x axis is perpendicular to the molecular plane and the z axis is the twofold symmetry axis. The calculations distinguish between the y and z in-plane axes, but this is not possible experimentally so that the experimental in-plane g values are listed as $g_\perp$ and $g_\perp'$.

Except for NCl_2, $g_{||}$ is very close to the free electron value ($g_e=2.0023$). There is good agreement between calculated and experimental values of $g_{||}$ for all the molecules. For a molecule with C_{2v} symmetry, no change in $g_{||}$ from g_e is indicated unless d orbitals are included.[2] The extended Hückel calculations show that the empty d orbitals are relatively closer to the unpaired electron molecular-orbital for NCl_2 than is the case for the other molecules, which explains the larger value of $g_{||}$ for NCl_2.

In the case of the in-plane g values, both $g_\perp$ and $g_\perp'$ exhibit the same trend[29]: An increase in g along the series PF_2, PCl_2, NF_2, and NCl_2. Thus, an increase in in-plane g value parallels a decrease in the difference in electronegativity between the central atom and the halogen (see Sec. V.C). For PF_2 and PCl_2 this difference is greater than one, and $g_\perp$ and $g_\perp'$ are both less than or equal to g_e and for NF_2 and NCl_2 the difference is less than one and $g_\perp$ and $g_\perp'$ are both greater than g_e. All the calculated in-plane g values (except for PF_2) are larger than the corresponding experimental values. The calculated values, however, do exhibit the same trend as the experimental ones.

It is difficult for us to rationalize from the nature of the extended Hückel calculations why this trend should exist. Perhaps further theoretical calculations of a more sophisticated type will reveal the origin of the observed effect.

ACKNOWLEDGMENTS

We want to thank Dr. D. Stedman and J. Burdett for samples of NCl_3 and $^{15}NCl_3$. Grateful acknowledgment is made to the National Science Foundation for their partial support of this research.

APPENDIX

The spin densities for a radical very rarely add up to unity. This is partly due to the difficulty in obtaining accurate reference values and is also due to the approximations inherent in converting experimental results into spin densities.[2] Two sets of reference values are in common usage, those compiled by Atkins and Symons[20] and ones calculated by Hurd and Coodin.[23] We have used the latter set to obtain the values reported in Table III resulting in total spin densities for PCl_2, NCl_2, PF_2, and NF_2 which are 1.01, 1.01, 1.09, and 1.04, respectively. If Atkins and Symons' reference values are used, these quantities become 1.29, 1.23, 1.38, and 1.22. Thus for each species the total spin density is considerably greater than unity when Atkins and Symons' values are used while Hurd and Coodin's values result in total spin densities much closer to one. On this basis, we conclude that the reference values calculated by Hurd and Coodin[23] are close to an optimal set and are preferred for use in estimating spin densities. Normalized spin densities for the radicals treated in this work are essentially identical regardless which set of reference values is used. This is because each of the values reported by Hurd and Coodin is approximately 25% higher than the ones collected by Atkins and Symons.

* Based in part on the dissertation of Michael S. Wei in partial fulfillment of the requirements for the Ph.D. degree in Chemistry from the University of Michigan, 1970.

† Present address: Gulf Research and Development Co., P.O. Drawer 2038, Pittsburgh, Pa. 15230.

[1] P. H. Kasai and E. B. Whipple, Mol. Phys. **9**, 497 (1965).

[2] M. S. Wei, J. H. Current, and J. Gendell, J. Chem. Phys. **52**, 1592 (1970).

[3] W. Nelson, G. Jackel, and W. Gordy, J. Chem. Phys. **52**, 4572 (1970).

[4] G. F. Kokoszka and F. E. Brinckman, J. Am. Chem. Soc. **92**, 1199 (1970).

[5] W. S. Metcalf, J. Chem. Soc. **1942**, 148.

[6] M. S. Wei, Ph.D. thesis, University of Michigan, Ann Arbor, Mich., 1970.

[7] A. E. Douglas and M. Frackowski, Can. J. Phys. **40**, 832 (1962).

[8] V. Vanderkook, Jr., and J. S. Mackenzie, Advan. Chem. Ser. **36**, 98 (1962).

[9] C. K. Jen, S. N. Foner, E. L. Cochran, and V. A. Bowers, Phys. Rev. **112**, 1169 (1958).

[10] R. L. Morehouse, J. J. Christiansen, and W. Gordy, J. Chem. Phys. **45**, 1747 (1966).

[11] P. H. Kasai, W. Weltner, Jr., and E. B. Whipple, J. Chem. Phys. **42**, 1120 (1965).

[12] P. H. Kasai, E. B. Whipple, and W. Weltner, Jr., J. Chem. Phys. **44**, 2581 (1966).

[13] J. Maruani, C. A. McDowell, H. Nakajima, and P. Raghunathan, Mol. Phys. **14**, 349 (1968).

[14] A. Hinchiffe and J. N. Murrell, Mol. Phys. **14**, 147 (1968).

[15] M. Karplus and G. K. Fraenkel, J. Chem. Phys. **35**, 1312 (1961).

[16] P. W. Atkins, J. A. Brivati, N. Keen, M. C. R. Symons, and P. A. Trevalion, J. Chem. Soc., **1962**, 4785.

[17] D. Stedman (personal communication).

[18] C. K. Jen, S. N. Foner, E. L. Cochran, and V. A. Bowers, Phys. Rev. **112**, 1169 (1958).
[19] J. K. Burdett and J. H. Current (personal communication, 1970).
[20] P. W. Atkins and M. C. R. Symons, *The Structure of Inorganic Radicals*, (Elsevier, New York, 1967).
[21] J. K. S. Wan, J. R. Morton, and H. J. Bernstein, Can. J. Chem. **44**, 1957 (1966).
[22] J. B. Farmer, M. C. L. Gerry, and C. A. McDowell, Mol. Phys. **8**, 253 (1964).
[23] C. M. Hurd and P. Coodin, J. Phys. Chem. Solid **28**, 523 (1967).
[24] L. S. Bartell, L. S. Su, and H. K. Yow, Inorg. Chem. **9**, 1903 (1970).
[25] P. Kisliuk and C. H. Townes, J. Chem. Phys. **18**, 1109 (1950).
[26] P. P. Stevenson and V. Schomaker, J. Am. Chem. Soc. **62**, 1913 (1940).
[27] H. J. Bower, M. C. R. Symons, and D. J. A. Tinling, *Radical Ions*, edited by E. Kaiser and L. Kevan, (Wiley-Interscience, New York, 1967), Chap. 10.
[28] L. Pauling, *The Na ure of the Chemical Bond* (Cornell U. P., Ithaca, N.Y., 1960).
[29] $g_\perp$ is associated with either the y or z molecular axes, but experimentally we cannot determine which one. The observed trend in $g_\perp$ and $g_\perp'$ values, however, exists regardless of the assignment of $g_\perp$ and $g_\perp'$ to molecular axes for each molecule.

THE JOURNAL OF CHEMICAL PHYSICS VOLUME 57, NUMBER 6 15 SEPTEMBER 1972

Spectrum of Exchange Coupled Cr^{3+} Pairs in $YAlO_3$

J. P. VAN DER ZIEL
Bell Telephone Laboratories, Incorporated, Murray Hill, New Jersey 07974
(Received 12 May 1972)

The optical spectrum and exchange splittings of the two types of nearest neighbor Cr^{3+} pairs in orthorhombic $YAlO_3$ have been studied. The emission spectrum from 7200 to 7350 Å yields the ground state exchange $-\mathbf{JS}\cdot\mathbf{S}+j(\mathbf{S}\cdot\mathbf{S})^2$ with $J_a=-24.7$, $j_a=-0.66$ cm^{-1} and $J_b=-26.2$ and $j_b=-0.91$ cm^{-1}. From the shift of the lines under uniaxial compression along the crystal z axis we conclude these values correspond, respectively, to pairs whose axes are in the xy plane and along the z axis. The energies of several pair levels with one ion in ^2E and the other in $^4A_2$, having $S=1$ and 2 have been obtained. Selective enhancement of *nn* pair luminescence is observed when the excitation energy is at about twice the single ion ^2E energy. The excitation and absorption spectra indicate these are pair levels corresponding to both ions in the ^2E state and have $S=0$ and 1. The single ion transitions are magnetic dipole in agreement with Cr^{3+} being at a center of inversion. The pair lines are electric dipole, and the strongest transitions in the infrared, and the pair lines in the ultraviolet obey the selection rule $\Delta S=0$ indicating the pair transitions obtain their intensity from the spin dependent dipole moment mechanism.

I. INTRODUCTION

The presence of Cr^{3+} pairs results in the appearance of additional lines in the single ion ^2E to $^4A_2$ luminescence spectrum. The pair spectrum is host dependent, and the importance of studying the pairs in a simple and well defined environment has recently been emphasized.[1] In the much studied case of $Al_2O_3:Cr^{3+}$ there are a large number of near neighbor types and the spectrum is exceedingly complex.[2] The spectrum of Cr^{3+} pairs in the perovskite structure and its distorted modifications is considerably simpler. In the trigonally distorted phase, exemplified by $LaAlO_3$, there is only one type of nearest neighbor pair with a large exchange interaction, and the pair system has recently been studied in detail.[1,3]

The spectrum of Cr^{3+} pairs in $YAlO_3$ discussed in this paper is somewhat more complex. The orthorhombic unit cell shown in Fig. 1 contains four $YAlO_3$ units, and the space group of the lattice is D_{2h}^{16}–$Pbnm$.[4] The four Al^{3+} sites, on which the Cr^{3+} ions substitute, have C_i site symmetry, and are labeled 1–4. The sites are equivalent except for the directions of the local site axes whose relative orientations can be obtained from the operations of the space group once the site axes of one of the sites are known.[5] Because of the low site symmetry the site axes are not simply related to the crystal axes.

There are four types of near neighbor (nn) pairs: two in the xy plane: 1–3, 2–4, and two along the z axis: 1–2, 3–4. The next nearest neighbor pairs are 1–4, 2–3. The crystal field splitting of isolated Cr^{3+} ions is the same for the four sites. For the nn pairs the crystal field can be different to the extent that the perturbation resulting from the substitution of a Cr^{3+} ion along the z axis is different from having a Cr^{3+} neighbor in the xy plane. Using the space group operations one can show that the pairs in the xy plane will have the same exchange splittings. Similarly, the exchange for the z-axis pairs will be equal but it is not required from symmetry arguments to be equal to the exchange of the xy plane pairs. There is only one near neighbor type in the cubic perovskite phase. Since the distortion in the orthorhombic phase is relatively small, the crystal field and exchange splittings of the xy plane and axial pair types will not be significantly different, and this is indeed observed.

The superexchange interaction between two Cr^{3+} ions